Eur. Phys. J. D (2018) 72: 31
https://doi.org/10.1140/epjd/e2017-80623-6

THE EUROPEAN PHYSICAL JOURNAL D

Regular Article

Hydrogen rearrangements in the fragmentation of anthracene by low-energy electron impact*

Peter J.M. van der Burgt[a], Melissa Dunne, and Marcin L. Gradziel

Department of Experimental Physics, National University of Ireland Maynooth, Maynooth, Co. Kildare, Ireland

Received 29 September 2017 / Received in final form 24 November 2017
Published online 6 February 2018 – © EDP Sciences, Società Italiana di Fisica, Springer-Verlag 2018

Abstract. We have measured mass spectra for positive ions produced by low-energy electron impact on anthracene using a reflectron time-of-flight mass spectrometer. The electron impact energy has been varied from 0 to 100 eV in steps of 0.5 eV. Ion yield curves of most of the fragment ions have been determined by fitting groups of adjacent peaks in the mass spectra with sequences of normalized Gaussians. Appearance energies for all these ions have been determined, and we report the first direct measurement of the triple ionization energy of anthracene at 45.5 ± 0.5 eV. The groups of fragments containing 8–13 carbon atoms provide evidence for hydrogen rearrangements during the fragmentation, involving retention or loss of one or two additional hydrogen atoms. Groups of fragments with 6 and 7 carbon atoms clearly show the presence of doubly-charged fragments. The smaller fragments with 1–4 carbon atoms all show broadened peaks, and these fragments may be partly or mostly due to energetic charge-separation fragmentations of doubly-charged anthracene.

1 Introduction

Polycyclic aromatic hydrocarbons (PAHs) have been studied extensively in recent years, because of their relevance in astrophysical processes and in environmental chemistry. The infrared spectra of most interstellar objects are dominated by emission bands that are commonly attributed to PAH molecules [1]. PAHs are susceptible to hydrogen attachment and are considered to play a key role as catalysts in the formation of molecular hydrogen in the interstellar medium [2,3]. PAHs are also considered as essential components in the pathway to the origin of life [4]. In the Earth's environment, PAHs are widespread pollutants generated by the combustion of organic materials, and are of concern because many PAHs have toxic, mutagenic and/or carcinogenic properties [5,6].

The topic of this paper is the fragmentation of the PAH anthracene ($C_{14}H_{10}$) induced by low-energy electron impact. Electron induced processes are of high relevance in a number of different areas. Many molecular species in the interstellar medium are assumed to be formed by chemical reactions within the ice mantles on interstellar dust grains caused by irradiation of ultraviolet light and cosmic rays. This irradiation releases many secondary electrons which may themselves induce chemical reactions [7]. Low-energy collisions of electrons with molecules are important elementary processes in gaseous environments such as discharges, gas lasers and the Earth's atmosphere [8], and in focused electron beam induced deposition [9].

Collision induced fragmentation of anthracene and other PAHs has been the focus of extensive research. Several groups have published mass spectra of anthracene at 70 eV electron energy [10–13] and have determined the ionization energy of anthracene [10,14]. Man et al. [15] have studied excitation of anthracene by electron impact. The mass spectra of singly-charged ions produced by doubly- and triply-charged anthracene molecules have been obtained at 70 eV [13] and at 100 eV [16] electron impact. At 70 eV the preferred routes for charge separation of doubly-charged anthracene ions lead to the singly-charged fragments CH_3^+, $C_2H_2^+$ and $C_3H_3^+$ [13], and this has also been observed with 40.8 eV photon impact [17].

Tobita et al. [18] have studied both electron and photon impact and have determined single and double ionization energies. Photoionization studies with synchrotron radiation and other light sources have been performed by Hagan and Eland [17], Jochims et al. [19,20], Ling and Lifshitz [21] and Mayer et al. [22]. A detailed fragmentation study of laser desorbed anthracene in intense laser fields was performed by Robson et al. [23], showing the presence of doubly and triply charged fragments in the mass spectra. Murakami et al. [24] have performed measurements with fs circularly polarized laser light. Using synchrotron radiation, Hartman et al. [25,26] have measured the ratios of doubly to singly-charged molecular parent ions for anthracene and other aromatic hydrocarbons. Wehlitz [27] has reviewed double photoionization of hydrocarbons and aromatic molecules.

* Contribution to the Topical Issue "Low Energy Positron and Electron Interactions", edited by James Sullivan, Ron White, Michael Bromley, Ilya Fabrikant, and David Cassidy.

[a] e-mail: peter.vanderburgt@mu.ie

Ion collisions with PAHs have been studied recently by several groups and we refer to the review paper by Gatchell and Zettergren [28] for a comprehensive discussion. Postma et al. [29] report anthracene mass spectra obtained by impact with keV H^+ and He^{2+} ions. Brédy et al. [30] have studied fragmentation of anthracene induced by collisions with 40 keV Ar^{8+} ions. Using a coincident detection technique they measured mass spectra of anthracene ions differentiated by the charge r ($1 \geq r \geq 4$) of the parent ion $C_{14}H_{10}{}^{r+}$. The mass spectra in both these papers show the clear presence of doubly-charged fragments.

The fragmentation of doubly-charged anthracene formed in double-charge-transfer reactions of singly-charged ions with neutral anthracene has been studied by Martin et al. [31] and Reitsma et al. [32]. Johansson et al. [33] have performed collision induced dissociation experiments of 50 keV anthracene cations colliding with xenon atoms and have performed density functional calculations on possible fragmentation pathways for the loss of C_2H_2. Holm et al. [34] and Rousseau et al. [35] have measured mass spectra produced by low-energy ions interacting with anthracene clusters.

Calculated ionization and dissociation energies are reported by Zakrzewski et al. [36], Kukhta et al. [37] and Holm et al. [38]. Sanz et al. [39] have calculated electron scattering cross sections from anthracene over the energy range 0.00001–10 000 eV. Postma et al. [40] have performed a molecular dynamics simulation of slow ion collisions with anthracene.

The focus of this article is on electron induced fragmentation processes in anthracene. In the following sections we give an overview of the experiment, the data acquisition and the data analysis. We then present our results and compare these with other research. The two main focal points of the discussion are the evidence for hydrogen rearrangements, and the identification of multiply charged fragments.

2 Experiment

The experimental set-up consists of a resistively heated oven producing an effusive beam of anthracene molecules, a pulsed electron beam, and a reflectron time-of-flight mass spectrometer, housed in three inter-connected and differentially pumped vacuum chambers. The set-up has been used before for the study of nucleobases [41–43].

The molecular beam of anthracene is generated by heating the oven containing anthracene powder (99% purity from Sigma–Aldrich) to a temperature of 100 °C. Molecules are effusing from a capillary (0.5 mm diameter and 4.5 mm length) in the oven and pass through a skimmer (1.2 mm diameter) into the collision chamber where they are collided with electrons.

The electron gun is pulsed at a rate of 8 kHz with a 0.3 μs pulse width. The energy resolution of the electron beam is about 0.8 eV FWHM. The electron gun has been optimised in pulsed mode by maximizing the current on the Faraday cup and ensuring that the current was independent of electron impact energy. In this way an electron beam has been obtained with a total current that was constant down to 15 eV and dropped to 60% at 8 eV.

Positively charged fragments are extracted into the mass spectrometer 0.05 μs after the electron pulse. A delay generator (Stanford Research Systems DG535) is used to synchronise the pulsing of the electron gun, the ion extraction voltage, and the start of the multichannel scaler (FastComtec 7886S).

Data acquisition is controlled by LabVIEW code, which ramps the electron impact energy in 0.5 eV steps, acquires mass spectra as a function of electron impact energy, and adds each mass spectrum to the data already accumulated. The full data set consists of a two-dimensional array of ion yield as a function of time-of-flight and of electron impact energy. After each scan of the electron impact energy, which takes about two hours, the full data set is written to a file. The data set used for this paper consists of 23 scans of the electron impact energy. Comparison of mass spectra taken before, during and after the data acquisition shows no sign of thermal decomposition or other undesired effects.

3 Data analysis

The data analysis is essentially the same as described in earlier papers [41–43]. The mass resolution in the mass spectra is $\Delta m/m = 0.004$ at 178 u at 100 eV. Above 34 u adjacent peaks in the mass spectra are not fully resolved, and ion yield curves have been extracted from the full data set by fitting groups of adjacent peaks with sequences of normalized Gaussians.

A remnant of water vapour in the vacuum system produces peaks at 16–18 u in the mass spectra. The 17 u and 18 u ion yield curves have been used for calibration of the incident electron energy by comparison with the recommended ionization cross sections for the production of H_2O^+ and OH^+ in Itikawa and Mason [44] (Tab. 11) in the range 10–40 eV. The estimated error in the calibration is ±0.2 eV.

Appearance energies (first onsets) have been determined by fitting an onset function $f(E) = c(E - E_0)^p$ convoluted with a Gaussian to each of the ion yield curves. For second onsets an additional term was included in the onset function.

4 Results and discussion

4.1 Mass spectra

In the remainder of this article we will identify groups of peaks in our mass spectra by the number of carbon atoms contained in the fragments. Group 14 is the parent ion group, containing the masses 174 u to 180 u. Group 7 contains half-integer masses, and this group contains singly-charged fragments with 7 carbon atoms and doubly-charged fragments with 14 carbon atoms. Figure 1 shows the mass spectrum of anthracene at 70 eV electron impact energy. The ions in group 14 have the highest abundance, followed by the ions in groups 7 and 6. The

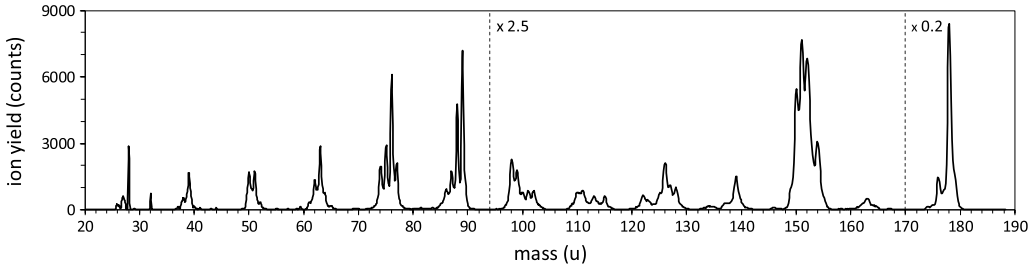

Fig. 1. The mass spectrum of anthracene at 70 eV electron impact energy. The peaks at 28 u and 32 u are due to a remnant of air in the vacuum chamber. For clarity, the ion yield between 94 u and 170 u is multiplied by 2.5, and the ion yield above 170 u is multiplied by 0.2. At 70 eV the yield in the parent ion group (172–180 u) is 45% of the total ion yield.

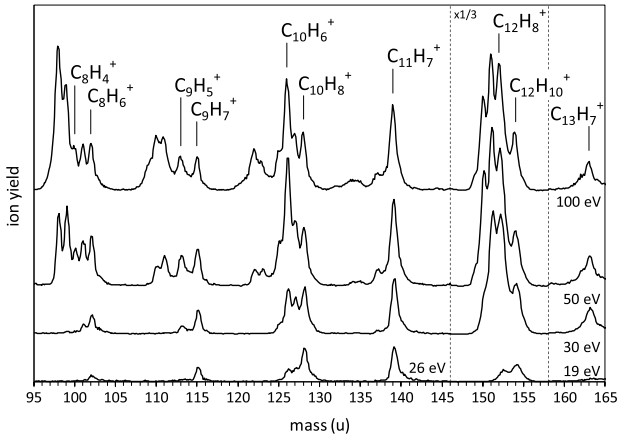

Fig. 2. Mass spectra of anthracene for the mass range 95–165 u, showing evidence for hydrogen rearrangements in the formation of fragments with 8–13 carbon atoms. The ion yield between 146 u and 158 u is scaled with a factor 1/3.

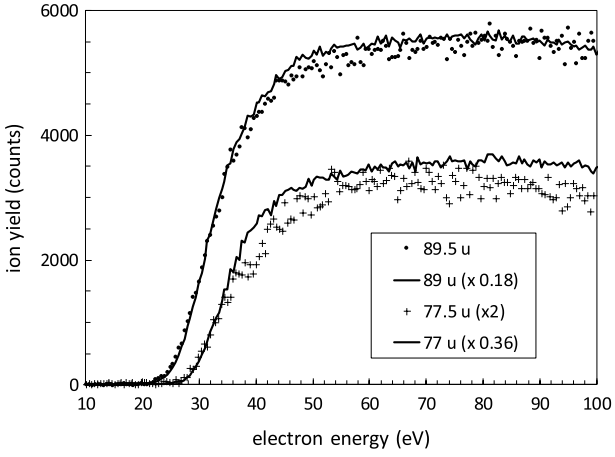

Fig. 3. Ion yield curves for 89.5 u, 89 u, 77.5 u, and 77 u. The only possible configurations for 89.5 u and 77.5 u are $C_{13}{}^{13}CH_{10}{}^{++}$ and $C_{11}{}^{13}CH_{10}{}^{++}$, respectively. The measured isotope ratio 179/178 u is 0.18 ± 0.01, which implies that 89 u is almost entirely $C_{14}H_{10}{}^{++}$, and 77 u is mostly $C_{12}H_{10}{}^{++}$. For further discussion see Section 4.1.

relative yields of ions in our mass spectrum at 70 eV compare reasonably well with those in Table 1 of Wacks and Dibeler [10], but for 39 u, 50–51 u, 74–75 u and 77 u we observe yields that are about 30% higher.

Evidence for hydrogen rearrangements is provided by some of the fragments in groups 8–13. Figure 2 shows the mass spectra for groups 8–13 at different electron impact energies. Fragmentation processes in relation to these groups are discussed in Section 4.3.

Evidence for the presence of doubly-ionized fragments is provided by peaks at half-integer masses in groups 6 and 7. 89 u and 77 u are mostly due to doubly-charged fragments. Groups 1 and 2 clearly show broadened peaks at integer masses, indicating that these are due to singly-charged fragments formed with a range of kinetic energies. Groups 3–5 feature broadened peaks of singly-charged fragments or peaks at non-integer masses due to multiply-charged fragments, or a combination of both. All these groups are discussed in Section 4.4.

Using femtosecond laser mass spectrometry, Robson et al. [23] have observed that the ratio of 89.5 u to 89 u is equal to the isotope ratio 179 u/178 u. Because the only possible configuration for 89.5 u is $C_{13}{}^{13}CH_{10}{}^{++}$, 89 u must be predominantly the doubly-charged parent. Postma et al. [29] have observed the same in ion-impact mass spectrometry. We observe that the 89.5 u/89 u and 179 u/178 u ratios are both equal to 0.18 ± 0.01, and are constant from 100 eV down to about 30 eV (below this energy statistical fluctuations in the 89.5 u ion yield affect the ratio). In Figure 3 the ion yield curves of 89 u and 89.5 u are compared, showing that both ion yield curves have the same shape within statistical error.

Wacks and Dibeler [10] observed that the 76.5 u/76 u ratio at 70 eV is equal to the isotope ratio, and deduced that the peaks in group 6 are primarily due to multiply charged ions. However, in our mass spectra the 76.5 u/76 u ratio = 0.22. The 77.5 u/77 u ratio is more relevant, because the only possible configuration for 77.5 u is $C_{11}{}^{13}CH_{10}{}^{++}$. We observe the 77.5 u/77 u ratio to be slightly lower than the isotope ratio and approximately constant between 30 and 100 eV. Figure 3 shows that the ion yield curves of 77 u and 77.5 u have nearly the same shape within statistical error.

4.2 Appearance energies

We have determined the appearance energies for most of the fragments of anthracene, and the results are listed in Table 1. The errors stated in Table 1 have been obtained

Table 1. Appearance energies and second onsets for anthracene fragments determined in this work.

Group	m/q (u)	Assignment	Appearance energy (eV)	Second onset (eV)
1	15	CH_3^+	17.7 ± 3.2	37.7 ± 1.0
2	26	$C_2H_2^+$	31.0 ± 0.6	
	27	$C_2H_3^+$	32.0 ± 0.8	
3	37	C_3H^+	44.1 ± 1.8	58.3 ± 1.4
	38	$C_3H_2^+$	34.9 ± 0.6	
	39	$C_3H_3^+$	21.0 ± 1.0	29.4 ± 1.3
	40	$C_3H_4^+$	32.9 ± 0.9	
4	49	C_4H^+	33.5 ± 0.9	60.3 ± 1.2
	50	$C_4H_2^+$	25.7 ± 1.1	31.7 ± 1.5
	51	$C_4H_3^+$	26.4 ± 1.4	30.9 ± 0.5
	52	$C_4H_4^+$	24.9 ± 1.1	30.8 ± 0.8
	53	$C_4H_5^+$	26.2 ± 1.0	
5	59.333	$C_{14}H_{10}^{+++}$	45.5 ± 0.5	
	61	$C_5H^+/C_{10}H_2^{++}$	39.5 ± 0.7	48.7 ± 1.2
	61.5	$C_{10}H_3^{++}$	44.9 ± 0.8	
	62	$C_5H_2^+/C_{10}H_4^{++}$	33.0 ± 0.6	37.9 ± 0.7
	62.5	$C_{10}H_5^{++}$	41.2 ± 0.7	
	63	$C_5H_3^+/C_{10}H_6^{++}$	26.0 ± 0.9	
	63.5	$C_{10}H_7^{++}$	35.0 ± 0.7	
	64	$C_5H_4^+/C_{10}H_8^{++}$	28.9 ± 1.0	33.7 ± 0.7
	64.5	$C_{10}H_9^{++}$	30.0 ± 0.6	
	65	$C_5H_5^+/C_{10}H_{10}^{++}$	26.9 ± 0.5	
6	73	C_6H^+	51.7 ± 1.3	
	74	$C_6H_2^+/C_{12}H_6^{++}$	28.5 ± 0.9	34.1 ± 0.8
	74.5	$C_{12}H_5^{++}$	31.3 ± 0.7	
	75	$C_6H_3^+/C_{12}H_6^{++}$	29.1 ± 0.5	
	75.5	$C_{12}H_7^{++}$	28.6 ± 0.6	37.6 ± 0.5
	76	$C_6H_4^+/C_{12}H_8^{++}$	27.2 ± 1.2	30.5 ± 0.5
	76.5	$C_{12}H_9^{++}$	29.2 ± 0.3	
	77	$C_{12}H_{10}^{++}/C_6H_5^+$	26.8 ± 0.3	
	77.5	$C_{11}{}^{13}CH_{10}^{++}$	27.4 ± 0.3	
	78	$C_6H_6^+$	26.2 ± 0.6	
7	84.5	$C_{14}H^{++}$	58.1 ± 1.7	
	85	$C_7H^+/C_{14}H_2^{++}$	30.0 ± 1.2	44.8 ± 1.2
	85.5	$C_{14}H_3^{++}$	47.6 ± 1.5	
	86	$C_7H_2^+/C_{14}H_{14}^{++}$	30.1 ± 0.8	35.3 ± 0.8
	86.5	$C_{14}H_5^{++}$	47.2 ± 1.0	
	87	$C_7H_3^+/C_{14}H_6^{++}$	26.2 ± 0.7	32.3 ± 0.6
	87.5	$C_{14}H_7^{++}$	36.8 ± 0.7	
	88	$C_7H_4^+/C_{14}H_8^{++}$	27.9 ± 1.0	30.9 ± 0.7
	88.5	$C_{14}H_9^{++}$	28.7 ± 0.7	35.3 ± 0.6
	89	$C_{14}H_{10}^{++}/C_7H_5^+$	20.2 ± 0.7	23.6 ± 0.6
	89.5	$C_{13}{}^{13}CH_{10}^{++}$	21.1 ± 0.5	24.3 ± 0.6
	90	$C_7H_6^+$	24.9 ± 0.4	
8	97	C_8H^+	46.9 ± 1.0	
	98	$C_8H_2^+$	29.9 ± 0.7	
	99	$C_8H_3^+$	27.4 ± 0.6	
	100	$C_8H_4^+$	29.8 ± 0.7	
	101	$C_8H_5^+$	26.4 ± 0.6	
	102	$C_8H_6^+$	22.9 ± 0.3	
	103	$C_8H_7^+$	22.0 ± 0.5	

(continued...)

Table 1. *(continued...)*

Group	m/q (u)	Assignment	Appearance energy (eV)	Second onset (eV)
9	109	C_9H^+	47.9 ± 0.8	
	110	$C_9H_2^+$	34.8 ± 0.6	
	111	$C_9H_3^+$	33.3 ± 0.6	
	112	$C_9H_4^+$	30.8 ± 0.8	
	113	$C_9H_5^+$	24.3 ± 0.3	
	114	$C_9H_6^+$	24.5 ± 0.5	
	115	$C_9H_7^+$	20.4 ± 0.2	
	116	$C_9H_8^+$	21.3 ± 0.6	
10	120	C_{10}^+	56.3 ± 0.6	
	121	$C_{10}H^+$	48.4 ± 0.6	
	122	$C_{10}H_2^+$	40.1 ± 0.7	
	123	$C_{10}H_3^+$	31.0 ± 0.7	
	124	$C_{10}H_4^+$	32.1 ± 0.6	
	125	$C_{10}H_5^+$	25.1 ± 0.5	
	126	$C_{10}H_6^+$	23.2 ± 0.2	26.3 ± 0.4
	127	$C_{10}H_7^+$	22.1 ± 0.3	
	128	$C_{10}H_8^+$	18.4 ± 0.3	
	129	$C_{10}H_9^+$	17.7 ± 0.5	
11	133	$C_{11}H^+$	52.2 ± 1.4	
	134	$C_{11}H_2^+$	39.9 ± 0.7	
	135	$C_{11}H_3^+$	40.6 ± 0.9	
	136	$C_{11}H_4^+$	(44 ± 4)	
	137	$C_{11}H_5^+$	25.3 ± 0.4	
	138	$C_{11}H_6^+$	24.3 ± 0.3	
	139	$C_{11}H_7^+$	17.8 ± 0.4	
	140	$C_{11}H_8^+$	20.1 ± 0.3	
12	149	$C_{12}H_5^+$	27.2 ± 0.6	
	150	$C_{12}H_6^+$	23.0 ± 0.2	
	151	$C_{12}H_7^+$	18.6 ± 0.2	
	152	$C_{12}H_8^+$	17.0 ± 0.2	
	153	$C_{12}H_9^+$	16.9 ± 0.2	
	154	$C_{12}H_{10}^+$	15.5 ± 0.2	
	155	$C_{11}{}^{13}CH_{10}^+$	16.4 ± 0.2	
13	161	$C_{13}H_5^+$	16.9 ± 1.0	
	162	$C_{13}H_6^+$	16.8 ± 0.5	
	163	$C_{13}H_7^+$	15.3 ± 0.6	
	164	$C_{13}H_8^+$	17.0 ± 0.9	
	165	$C_{13}H_9^+$	16.0 ± 0.3	
14	174	$C_{14}H_6^+$	28.2 ± 0.4	
	175	$C_{14}H_7^+$	25.7 ± 0.5	
	176	$C_{14}H_8^+$	17.3 ± 0.3	
	177	$C_{14}H_9^+$	16.5 ± 0.4	
	178	$C_{14}H_{10}^+$	7.4 ± 0.2	
	179	$C_{13}{}^{13}CH_{10}^+$	7.3 ± 0.4	
	180	$C_{12}{}^{13}C_2H_{10}^+$	9.2 ± 0.3	

directly from the Levenberg–Marquardt algorithm used for the fitting of the onset function; the uncertainty in the calibration of the incident electron energy is not included in these errors.

The energy intervals used in the fitting range from about 10 eV to about 30 eV, in each case depending on the range of upward curvature of the ion yield curve. Figure 4 shows the fitted onset functions for six anthracene fragments that are relevant for the discussion in Section 4.3.

The appearance energy of the parent ion at 178 u is 7.4 ± 0.2 eV, in good agreement with earlier results [18,19,36–38,45].

The appearances energies of 89 u and of 89.5 u are 20.2 ± 0.7 eV and 21.1 ± 0.5 eV, respectively. Taking

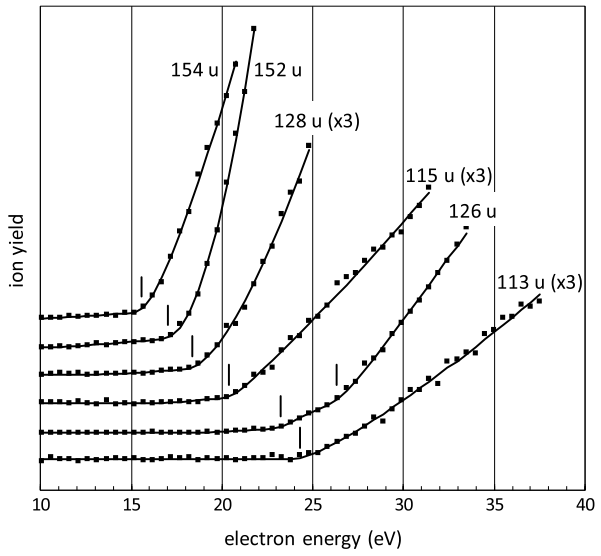

Fig. 4. Ion yield curves for six anthracene fragments. The locations of the appearance energies, the second onset for 126 u, and the fitted onset functions are also shown.

the weighted average, the double-ionization energy for anthracene is determined to be 20.8 ± 0.4 eV. Table 2 shows that this value compares well with several other determinations, but the photon impact values and the density functional theory (DFT) calculation are significantly lower. This has been noted and commented on earlier by Tobita et al. [18]. The 89 u and 89.5 u ion yield curves both have a second onset, at 23.6 ± 0.6 eV and 24.3 ± 0.6 eV, respectively, indicating the existence of a second fragmentation process with an onset at 24.0 ± 0.4 eV.

Directly to the left of the 60 u peak in group 5 is a small but distinct peak at 59.33 u. This is attributed to the triply-charged parent molecule. Figure 5 shows a small part of the mass spectrum, the ion yield curve, and the fitted onset function for the triply-charged parent. The appearance energy is 45.5 ± 0.5 eV. This is the first direct determination of the triple ionization energy. Our value is significantly higher than the measurement of 38.2 eV by Kingston et al. [13], see Table 2, who determined the double and triple ionization energies from energy defects in the charge stripping reactions of multiply-charged parent ions in N_2 gas. Our value is also much higher than the DFT value from Holm et al. [38].

Table 3 compares the appearance energies for six fragments obtained by H, H_2, C_2H_2, C_2H_3, C_3H_3 and C_4H_2 losses. Our values are systematically higher than those of Ling and Lifshitz [21], but reasonable agreement is obtained with the values for Jochims et al. [19]. The values for 177 u and 176 u show that H loss and H_2 loss require substantial amounts of energy, and this has also been observed for other small PAHs [46,47]. Notably, the appearance energies for 177 u and 176 u are very similar, and are 16.5 ± 0.4 eV and 17.3 ± 0.3 eV, respectively.

The 175 u and 174 u fragments have very low yields, and have appearance energies of 25.7 ± 0.5 eV and 28.2 ± 0.4 eV, respectively (see Tab. 1), showing that the loss of three and four hydrogen atoms requires even more energy. The appearance energies for 177 u to 174 u indicate a pairing effect, and suggest that 176 u is formed by H_2 loss , 175 u is formed by H_2 + H loss, and 174 u is formed by H_2 + H_2 loss. This may be of interest in relation to the contribution of PAHs to the formation of cosmic H_2 [2].

In general, the appearance energies for the fragments in groups 8–13 are progressively higher for smaller groups, and within each group appearance energies tend to be higher for fragments with fewer hydrogen atoms. This indicates that at higher electron impact energies excess excitation energy is lost by the release of additional hydrogen atoms. In the groups 9, 10 and 12 the lowest appearance energies are observed for 115 u (C_5H_3 loss), 128 u (C_4H_2 loss) and 154 u (C_2 loss), indicating that transfer of one or two hydrogens atoms during the fragmentation is energetically favorable. This is discussed in more detail in Section 4.3. Between 15 and 20 eV, several of the fragments in groups 10–13 have appearance energies below the double ionization energy, showing that these fragments are produced by singly-charged anthracene.

With the exception of 89 u and 89.5 u, in groups 4–7 all appearance energies are 24.9 eV or higher, well above the double ionization energy of anthracene. Within each group appearance energies tend to be higher for fragments with fewer hydrogen atoms. This raises the question to what extent the ions in these groups originate from double ionization of anthracene (see discussion in Sect. 4.4).

Assuming that the 89 u, 88 u, 76 u and 75 u fragments in our mass spectra are largely due to doubly charged ions, we can compare our appearance energies with those obtained by Mathur et al. [16] from doubly-charged ion mass spectrometry. Table 4 lists the values. There is some similarity in the values for three of the ions, but the appearance energy for $C_{14}H_8{}^{2+}$ from [16] is surprisingly low given the large difference in appearance energy between 178 u and 176 u.

In groups 1–3 the fragments with the highest yields at 100 eV are 39 u, 38 u, 27 u, 26 u, 37 u, and 15 u. These fragments have been identified as singly-charged products of charge separation processes in multiply charged ions [13,17,30]. All these fragments are appearing as broadened peaks in our mass spectra at energies above about 35 eV. At 100 eV, the sum of the yields of all ions in groups 1–3 is only 6.6% of the total ion yield.

The appearance energy for 39 u is 21.0 ± 1.0 eV, which is equal to the double ionization energy of anthracene. A second onset is observed at 29.4 ± 1.3 eV. Possibly the first onset at 21.0 eV is due to fragmentation of singly-charged anthracene, whereas the second onset is due to fragmentation of doubly-charged anthracene. The appearance energies for the other ions in group 3 are much higher.

The appearance energies for 26 u and 27 u in group 2 are higher than for most other fragments. The fragments in group 1 have very low yields; we only obtained an appearance energy for 15 u at 17.7 ± 3.2 eV.

Table 2. Comparison of double and triple ionization energies.

Reference	Method	Double ionization	Triple ionization
Present work	Electron impact	20.8 ± 0.4 eV	45.5 ± 0.5 eV
Wacks and Dibeler [10]	Electron impact	21.1 ± 0.5	
Kingston et al. [13]	Mass spectrometry[1]	21.2	38.2
Mathur et al. [16]	Electron impact	21.1 ± 0.5	
Tobita et al. [18]	Electron impact[2]	21.1 ± 0.2	
Hartman et al. [26]	Photon impact	20.07 ± 0.17	
Tobita et al. [18]	Photon impact[2]	19.6 ± 0.2	
Wacks and Dibeler [10]	Group equiv. method	20.4	
Holm et al. [38]	DFT calculation[3]	19.04	36.22

[1] Values obtained from Table 4.
[2] On anthracene-d10.
[3] Vertical ionization energies obtained from Table 2.

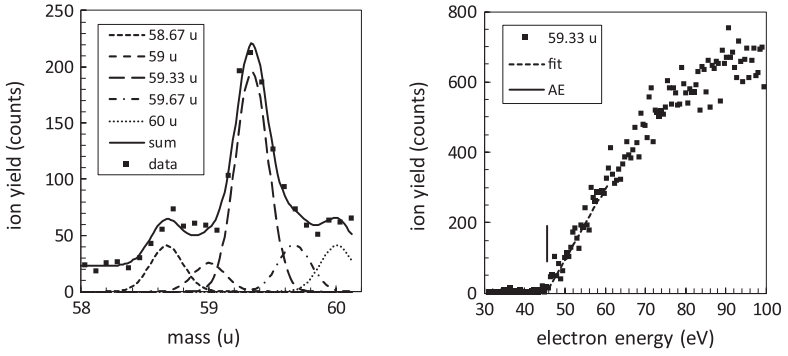

Fig. 5. Left: 58–60 u mass spectrum at 100 eV, showing a fit with third-integer peaks. Right: ion yield curve for 59.33 u and determination of the appearance energy at AE = 45.5 ± 0.5 eV.

Table 3. Comparison of appearance energies of singly-ionized fragments.

Ion	m/q	Present work Electron impact	Jochims et al. [19] Synchr. rad.[1]	Ling and Lifshitz [21] UV photo ion[2]	Holm et al. [38] DFT calculation[3]
$C_{10}H_8^+$	128 u	18.4 ± 0.3 eV		15.4 ± 0.2 eV	
$C_{11}H_7^+$	139	17.8 ± 0.4		14.8 ± 0.3	
$C_{12}H_7^+$	151	18.6 ± 0.2		17.4 ± 0.2	
$C_{12}H_8^+$	152	17.0 ± 0.2	16.00 ± 0.15 eV	15.2 ± 0.2	10.44 eV
$C_{14}H_8^+$	176	17.3 ± 0.3	17.31 ± 0.10	15.8 ± 0.2	
$C_{14}H_9^+$	177	16.5 ± 0.4	15.79 ± 0.10	15.0 ± 0.2	12.44

[1] On anthracene-d10.
[2] Values from Table 1, for 24 μs ion trap storage time.
[3] Values obtained from Tables 2 and 5.

4.3 Groups 8–13: evidence for hydrogen rearrangements

4.3.1 Groups 11 and 13

The peaks in group 13 have low yields and appearance energies around 16 eV. The most abundant fragment is 163 u, with an appearance energy of 15.3 ± 0.6 eV, attributed to CH_3 loss. 165 u (CH loss) has a slightly higher appearance energy of 16.0 ± 0.3 eV, and a lower ion yield compared to 163 u, indicating that CH_3 loss is favoured to CH loss.

Kingston et al. [13] have proposed several reaction schemes for the formation of charge separation products from doubly-charged anthracene. Their Scheme 3 involves the opening of one of the terminal rings resulting in a side chain with three carbon atoms. Migration of two hydrogen atoms to the end of the side chain is then followed by charge separation producing $C_{13}H_7^+ + CH_3^+$. A similar mechanism may well be responsible for the fragmentation $C_{13}H_7^+ + CH_3$. In our mass spectra the 15 u fragment (CH_3^+) has a very low yield with an appearance energy of 17.7 ± 3.2 eV, indicating that the same fragmentation with charge localization on the smaller fragment may also be a possibility.

The most abundant fragment in group 11 is 139 u, with an appearance energy of 17.8 ± 0.4 eV. This fragment is attributed to C_3H_3 loss by the breaking of two C–C bonds. Scheme 4 of Kingston et al. [13] involving the opening of a terminal ring, the rearrangement of end three carbon

Table 4. Comparison of appearance energies of doubly-ionized fragments.

Ion	m/q	Present work	Mathur et al. [16]
$C_{12}H_6^{++}$	75 u	29.1 ± 0.5 eV	31.8 ± 0.5 eV
$C_{12}H_8^{++}$	76	27.2 ± 1.2	29.9 ± 0.5
$C_{14}H_8^{++}$	88	27.9 ± 1.0	21.2 ± 0.5
$C_{14}H_{10}^{++}$	89	20.2 ± 0.7	21.1 ± 0.5

atoms, and the formation of cyclopropenyl may well apply here.

The other fragments in group 11 have low yields and higher appearance energies. The lowest mass fragment in this group is 132 u, attributed to C_{11}^+. Noticeably, the peak at 136 u is almost absent, indicating that $C_3H_3 + 3H$ loss is unlikely.

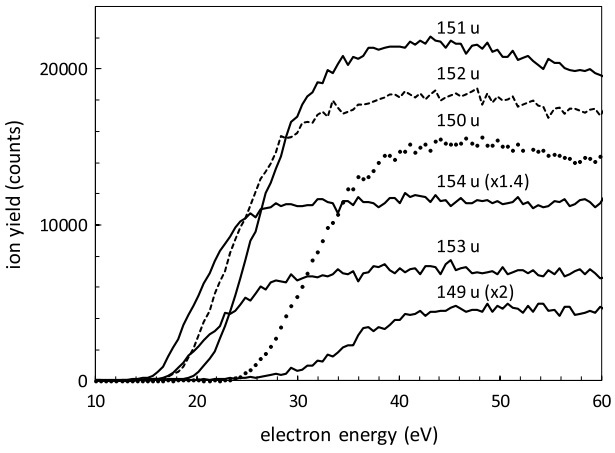

Fig. 6. Ion yield curves for the fragments of group 12. $C_{12}H_{10}^+$ (154 u) has a lower appearance energy than $C_{12}H_8^+$ (152 u), C_2 loss is more likely than C_2H_2 loss.

4.3.2 Groups 8, 9, 10 and 12

If one would assume that the most abundant fragment in group 12 would be formed by the breakage of two C–C bonds in one of the terminal rings, one would expect that 152 u ($C_{12}H_8^+$ formed by C_2H_2 loss) would have the highest yield and the lowest appearance energy. At higher electron energies 152 u and 151 u are the fragments with the highest abundance in this group, but 154 u has the lowest appearance energy of 15.5 ± 0.2 eV, indicating that the transfer of two hydrogen atoms during the fragmentation resulting in C_2 loss is energetically favorable at low electron energies.

The fitted onset functions for 154 u and 152 u are shown in Figure 4. Ion yield curves for the ions in group 12 are shown in Figure 6, clearly showing that between 16 and 24 eV, C_2 loss is the most likely fragmentation. The ratio 155 u/154 u is approximately equal to the isotope ratio 179 u/178 u, and 155 u is attributed to C_2 loss from the anthracene isotope. C_2H_2 loss is a prominent fragmentation of naphthalene, but C_2 loss has not been reported [10,47].

A mechanism similar to Scheme 2 of Kingston et al. [13] may be responsible for C_2H_2 loss with the formation of 152 u. This involves the opening of a terminal ring with a side chain containing four carbon atoms, followed by breakage of the C–C bond in the centre of the side chain, yielding singly-charged 2-ethynylnaphtalene. Possibly hydrogen migration from the side chain towards the main fragment could then explain the formation of 154 u with C_2 loss.

Johansson et al. [33] have performed DFT calculations for the loss of C_2H_2 from singly-charged anthracene, and have identified three fragmentation pathways proceeding via several intermediate configurations. One of these pathways yields singly-charged 2-ethynylnaphtalene. Reitsma et al. [32] show the result of a DFT calculation for the loss of C_2H_2 from doubly-charged anthracene, where C_2H_2 emission occurs after isomerization to benz[a]azulene.

In group 10, one would expect that 126 u ($C_{10}H_6^+$ formed by C_4H_4 loss from one of the terminal rings at an appearance energy of 23.2 ± 0.2 eV) would have the highest yield and the lowest appearance energy. This is indeed the fragment with the highest abundance at higher electron energies, but 128 u has an appearance energy that is 4.8 eV lower (18.4 ± 0.3 eV), indicating that the transfer of two hydrogen atoms during the fragmentation is energetically favorable at low electron energies. The ion yield curves are shown in Figure 7. 127 u has an appearance energy at 22.1 ± 0.3 eV, slightly lower than 126 u. 129 u, with an appearance energy at 17.7 ± 0.5 eV, is attributed to C_4H_2 loss from the anthracene isotope. We note that in the mass spectrum of phenanthrene at 21.21 eV photon energy 128 u is present, but 126 u is absent (Fig. 2 in [21]).

Jochims et al. [47] have proposed that C_4H_2 loss from naphthalene proceeds by the formation of a biradical form of $C_{10}H_8^+$ followed by fragmentation into the benzene cation and C_4H_2 as diacetylene. Similarly, C_4H_2 loss from anthracene could lead to the formation of the naphthalene cation. This has also been proposed by Ling and Lifshitz [21].

In group 9, the loss of a fragment with 5 carbon atoms requires the breakage of three C–C bonds in both the central ring and one of the terminal rings. Without hydrogen rearrangement, C_5H_4 loss would then be the most likely, producing $C_9H_6^+$ (114 u). However, $C_9H_7^+$ (115 u) has a lower appearance energy, and a higher abundance below 40 eV, indicating that the formation of 115 u involves the rearrangement of one hydrogen atom. At higher energies, the 112 u and 114 u fragments have lower abundances than 109, 110, 111, 113 and 115 u. Figure 8 shows the ion yield curves for this group (for clarity the 112 u ion yield curve is not included).

Breakage of two C–C bonds in the central ring could lead to C_6H_4 loss, producing $C_8H_6^+$ (102 u). This is indeed the fragment with the lowest appearance energy in group 8. At higher energies loss of additional hydrogen atoms become increasingly more likely. 103 u is attributed to C_6H_4 loss from the anthracene isotope.

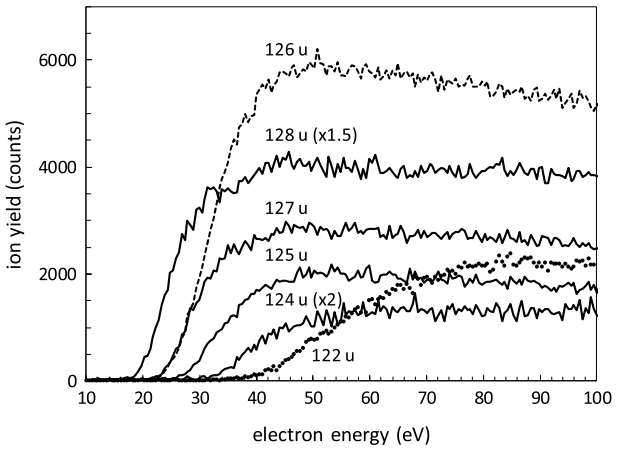

Fig. 7. Ion yield curves for the fragments of group 10. $C_{10}H_8^+$ (128 u) has a lower appearance energy than $C_{10}H_6^+$ (126 u), indicating that near threshold C_4H_2 loss is more likely than C_4H_4 loss.

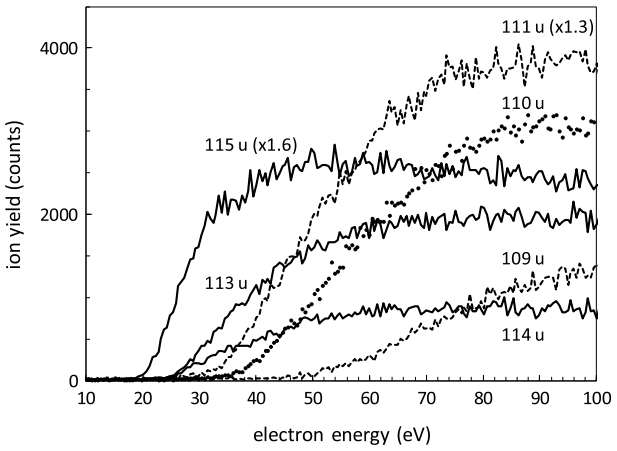

Fig. 8. Ion yield curves for the fragments of group 9. $C_9H_7^+$ (115 u) has a lower appearance energy than $C_9H_5^+$ (113 u), indicating that near threshold C_5H_3 loss is more likely than C_5H_5 loss.

4.4 Groups 1–7: evidence for multiple ionization

Examining the mass spectra of anthracene at different electron energies clearly shows evidence for multiple ionization. Groups 6 and 7 clearly show evidence for double ionization (see discussion in Sect. 4.1), and good fits were obtained by including half-integer peaks in the modelling of these groups with normalized Gaussians. We have also used half-integer peaks for the fitting of group 5.

Groups 3 and 4 feature broadened peaks of singly-charged fragments or peaks at non-integer masses due to multiply-charged fragments, or a combination of both. We found that good fits were obtained by using third-integer peaks, but these peaks are appearing well below 45.5 eV, so they cannot be due to triply-charged fragments. Groups 3 and 4 are therefore attributed to singly-charged fragments formed with a range of kinetic energies. The ion yield curves for the masses in groups 3 and 4 were obtained by adding the third-integer yields to the yield of the nearest integer peak (for example, the 38.67 u, 39 u and 39.33 u yields were added to obtain the ion yield curve for 39 u).

Groups 1 and 2 only clearly show the presence of peaks at 15 u, 26 u and 27 u. Very small peaks occur at 12 u, 13 u and 25 u. At higher electron energies all these peaks are broadened and there are no indications of half-integer peaks. (Peaks at 14 u and 28 u are due to a remnant of nitrogen in the vacuum chamber.) Ion yield curves for these peaks were determined by summing counts over appropriate bin ranges.

In groups 1–5, with the exception of 15 u and 39 u, all appearance energies are over 5 eV higher than the double ionization energy of anthracene. This raises the question to what extent the masses in these groups are due to doubly-ionized fragments.

Brédy et al. [30] have studied fragmentation of anthracene in collisions with 40 keV Ar^{8+} ions. They used a coincident detection technique to measure mass spectra of anthracene ions differentiated by the charge r ($1 \geq r \geq 4$) of the parent ion $C_{14}H_{10}{}^{r+}$. In the mass spectrum for the $C_{14}H_{10}{}^{2+}$ parent, the ions in groups 6 and 7 are predominant, but the groups 2–5 have low abundance. In the mass spectrum for the $C_{14}H_{10}{}^{3+}$ parent, the peak corresponding to the parent is the largest.

In our mass spectra the triply-charged parent has a very low abundance, indicating that the doubly-charged fragments must be coming mostly from the doubly-charged parent, and that groups 6 and 7 are mostly doubly-charged fragments, but singly-charged fragments contribute to the groups with the smaller masses. Groups 1–4 feature broadened peaks of singly-charged fragments produced in part by charge separation of doubly-charged anthracene. Group 5 may be a mixture of singly- and doubly-charged fragments.

5 Conclusions

We have determined the appearance energies for most fragments of anthracene, produced by low-energy electron impact, and this includes the first direct determination of the triple-ionization energy of anthracene.

The appearance energies of 177 u to 174 u are substantially higher than the single ionization energy of anthracene, and indicate a pairing effect suggesting that 176 u is formed by H_2 loss and 174 u is formed by $H_2 + H_2$ loss.

The groups of fragments containing 8–13 carbon atoms provide evidence for hydrogen rearrangements during the fragmentation. We have found several indications for retention or loss of one or two additional hydrogen atoms. Several of the fragments in groups 10–13 have appearance energies below the double ionization energy of anthracene, and there is no substantial broadening of the peaks at higher electron energies. These fragments are mostly or entirely produced by singly-charged anthracene, but at higher electron energies there may be some contribution from the fragmentation of doubly-charged anthracene.

The groups of fragments with 1–7 carbon atoms provide evidence for multiple ionization. Groups 6 and 7 clearly show the presence of doubly-charged fragments.

Based on the isotope ratio we have concluded that 89 u is almost entirely $C_{14}H_{10}{}^{++}$, and 77 u is mostly $C_{12}H_{10}{}^{++}$. Group 5 is possibly partly attributable to doubly-charged fragments and partly to singly-charged fragments from charge separation reactions of doubly-charged anthracene. Groups 1–4 all show broadened peaks. The high appearance energies and relatively low abundances indicate that these fragments may be partly or mostly due to energetic charge-separation fragmentations of doubly-charged anthracene.

Following the measurements on anthracene, we acquired a full dataset of 200 mass spectra for phenanthrene. Comparison of the mass spectra of phenanthrene and anthracene by stepping through all electron energies does not reveal any clear systematic difference, and we suspect that there are no substantial differences in the electron-induced fragmentation pathways between anthracene and phenanthrene.

The authors wish to acknowledge Mr. David Watson for his contributions to the mechanical design of the apparatus, and to Mr. Pat Seery for his contributions to the electronics equipment.

Author contribution statement

The measurements were performed by PvdB with help from MD. MG provided essential contributions to the data acquisition. The analysis of the data was done by MD and PvdB. PvdB wrote the paper, and all the authors contributed to the discussion of the results.

References

1. A.G.G.M. Tielens, Rev. Mod. Phys. **85**, 1021 (2013)
2. S. Cazaux, L. Boschman, N. Rougeau, G. Reitsma, R. Hoekstra, D. Teillet-Billy, S. Morisset, M. Spaans, T. Schlathölter, Sci. Rep. **6**, 19835 (2016)
3. T. Chen, M. Gatchell, M.H. Stockett, R. Delaunay, A. Domaracka, E.R. Micelotta, A.G.G.M. Tielens, P. Rousseau, L. Adoui, B.A. Huber, H.T. Schmidt, H. Cederquist, H. Zettergren, J. Chem. Phys. **142**, 144305 (2015)
4. J. Groen, D.W. Deamer, A. Kros, P. Ehrenfreund, Orig. Life Evol. Biosph. **42**, 295 (2012)
5. A.T. Lawal, Cogent Environ. Sci. **3**, 1339841 (2017)
6. K.-H. Kima, S.A. Jahan, E. Kabir, R.J.C. Brown, Environ. Int. **60**, 71 (2013)
7. N.J. Mason, B. Nair, S. Jheeta, E. Szymańska, Faraday Discuss. **168**, 235 (2014)
8. R. Balog, J. Langer, S. Gohlke, M. Stano, H. Abdoul-Carime, E. Illenberger, Int. J. Mass Spectr. **233**, 267 (2004)
9. R.M. Thorman, T.P. Ragesh Kumar, D.H. Fairbrother, O. Ingólfsson, J. Beilstein, Nanotechnology **6**, 1904 (2015)
10. M.E. Wacks, V.H. Dibeler, J. Chem. Phys. **31**, 1557 (1959)
11. R.C. Dougherty, C.R. Weisenberger, J. Am. Chem. Soc. **90**, 23 (1968)
12. B. Shushan, R.K. Boyd, Org. Mass Spectrom. **15**, 445 (1980)
13. R.G. Kingston, M. Guilhaus, A.G. Brenton, J.H. Beynon, Org. Mass Spectrom. **20**, 406 (1985)
14. H. Kuroda, Nature **201**, 1214 (1964)
15. K.F. Man, S. Trajmar, J.W. McConkey, J.M. Ratliff, M. Khakoo, J. Phys. B: At. Mol. Opt. Phys. **25**, 5245 (1992)
16. B.P. Mathur, E.M. Burgess, D.E. Bosfwick, T.F. Moran, Org. Mass Spectrom. **16**, 92 (1981)
17. D.A. Hagan, J.H.D. Eland, Rapid Commun. Mass Spectrom. **5**, 512 (1991)
18. S. Tobita, S. Leach, H.W. Jochims, E. Rühl, E. Illenberger, H. Baumgärtel, Can. J. Phys. **72**, 1060 (1994)
19. H.W. Jochims, E. Rühl, H. Baumgärtel, S. Tobita, S. Leach, Astrophys. J. **420**, 307 (1994)
20. H.W. Jochims, H. Baumgärtel, S. Leach, Astrophys. J. **512**, 500 (1999)
21. Y. Ling, Ch. Lifschitz, J. Phys. Chem. A **102**, 708 (1998)
22. P.M. Mayer, V. Blanchet, Ch. Joblin, J. Chem. Phys. **134**, 244312 (2011)
23. L. Robson, A.D. Tasker, K.W.D. Ledingham, P. McKenna, T. McCanny, C. Kosmidis, P. Tzallas, D.A. Jaroszynski, D.R. Jones, Int. J. Mass Spectrom. **220**, 69 (2002)
24. M. Murakami, M. Tanaka, T. Yatsuhashi, N. Nakashima, J. Chem. Phys. **126**, 104304 (2007)
25. T. Hartman, P.N. Juranić, K. Collins, B. Reilly, N. Appathurai, R. Wehlitz, Phys. Rev. Lett. **108**, 023001 (2012)
26. T. Hartman, P.N. Juranić, K. Collins, B. Reilly, E. Makoutz, N. Appathurai, R. Wehlitz, Phys. Rev. A **87**, 063403 (2013)
27. R. Wehlitz, J. Phys. B: At. Mol. Opt. Phys. **49**, 222004 (2016)
28. M. Gatchell, H. Zettergren, J. Phys. B: At. Mol. Opt. Phys. **49**, 162001 (2016)
29. J. Postma, S. Bari, R. Hoekstra, A.G.G.M. Tielens, T. Schlathölter, Astrophys. J. **708**, 435 (2010)
30. R. Brédy, C. Ortéga, M. Ji, J. Bernard, L. Chen, G. Montagne, S. Martin, Phys. Scr. **T156**, 014042 (2013)
31. S. Martin, L. Chen, R. Brédy, G. Montagne, C. Ortega, T. Schlathölter, G. Reitsma, J. Bernard, Phys. Rev. A **85**, 052715 (2012)
32. G. Reitsma, H. Zettergren, S. Martin, R. Brédy, L. Chen, J. Bernard, R. Hoekstra, T. Schlathölter, J. Phys. B: At. Mol. Opt. Phys. **45**, 215201 (2012)
33. H.A.B. Johansson, H. Zettergren, A.I.S. Holm, N. Haag, S. Brøndsted Nielsen, J.A. Wyer, M.-B.S. Kirketerp, K. Støchkel, P. Hvelplund, H.T. Schmidt, H. Cederquist, J. Chem. Phys. **135**, 084304 (2011)
34. A.I.S. Holm, H. Zettergren, H.A.B. Johansson, F. Seitz, S. Rosén, H.T. Schmidt, A. Ławicki, J. Rangama, P. Rousseau, M. Capron, R. Maisonny, L. Adoui, A. Méry, B. Manil, B.A. Huber, H. Cederquist, Phys. Rev. Lett. **105**, 213401 (2010)
35. P. Rousseau, A. Ławicki, A.I.S. Holm, M. Capron, R. Maisonny, S. Maclot, E. Lattouf, H.A.B. Johansson, F. Seitz, A. Méry, J. Rangama, H. Zettergren, S. Rosén, H.T. Schmidt, J.-Y. Chesnel, A. Domaracka, B. Manil, L. Adoui, H. Cederquist, B.A. Huber, Nucl. Instrum. Meth. Phys. Res. B **279**, 140 (2012)
36. V.G. Zakrzewski, O. Dolgounitcheva, J.V. Ortiz, J. Chem. Phys. **105**, 8748 (1996)

37. A.V. Kukhta, I.N. Kukhta, N.A. Kukhta, O.L. Neyra, E. Meza, J. Phys. B: At. Mol. Opt. Phys. **41**, 205701 (2008)
38. A.I.S. Holm, H.A.B. Johansson, H. Cederquist, H. Zettergren, J. Chem. Phys. **134**, 044301 (2011)
39. A.G. Sanz, M.C. Fuss, F. Blanco, F. Carelli, F. Sebastianelli, F.A. Gianturco, G. García, Appl. Rad. Isotopes **83**, 68 (2014)
40. J. Postma, R. Hoekstra, A.G.G.M. Tielens, T. Schlathölter, Astrophys. J. **783**, 61 (2014)
41. P.J.M. van der Burgt, Eur. Phys. J. D **68**, 135 (2014)
42. P.J.M. van der Burgt, F. Mahon, G. Barrett, M.L. Gradziel, Eur. Phys. J. D **68**, 151 (2014)
43. P.J.M. van der Burgt, S. Finnegan, S. Eden, Eur. Phys. J. D **69**, 173 (2015)
44. Y. Itikawa, N. Mason, J. Phys. Chem. Ref. Data **34**, 1 (2005)
45. NIST Chemistry WebBook table of ionization energy determinations for anthracene, http://webbook.nist.gov/cgi/inchi?ID=C120127&Mask=20
46. Y. Gotkis, M. Oleinikova, M. Naor, Ch. Lifshitz, J. Chem. Phys. **97**, 12282 (1993)
47. H.W. Jochims, H. Rasekh, E. Rühl, H. Baumgärtel, S. Leach, Chem. Phys. **168**, 159 (1992)